

## Full length article

## Non-uniform phase separation in ferrite of a duplex stainless steel

B. Zhang<sup>a</sup>, F. Xue<sup>c</sup>, S.L. Li<sup>d</sup>, X.T. Wang<sup>e</sup>, N.N. Liang<sup>a</sup>, Y.H. Zhao<sup>a</sup>, G. Sha<sup>a, b, \*</sup><sup>a</sup> School of Materials Science and Engineering, Nanjing University of Science and Technology, Nanjing, 210094, China<sup>b</sup> Herbert Gleiter Institute of Nanoscience, Nanjing University of Science and Technology, Nanjing, 210094, China<sup>c</sup> Suzhou Nuclear Power Research Institute, China Guangdong Nuclear Group, Suzhou, 215004, China<sup>d</sup> State Key Laboratory for Advanced Metals and Materials, University of Science and Technology Beijing, Beijing, 100083, China<sup>e</sup> Collaborative Innovation Center of Steel Technology, University of Science and Technology Beijing, Beijing, 100083, China

## ARTICLE INFO

## Article history:

Received 17 March 2017

Received in revised form

5 June 2017

Accepted 21 August 2017

Available online 25 August 2017

## Keywords:

Duplex stainless steel

Phase separation

Interface

Heterogeneous nucleation

Atom probe tomography

## ABSTRACT

Phase separation in ferrite of a duplex stainless steel during aging at 400 °C for up to 20,000 h has been found to be non-uniform in nature by using atom probe tomography. Aging-induced segregation of Ni takes place strongly at the austenite/ferrite interfaces accompanied by the formation of Ni depletion zones (NDZs) in the ferrite in the vicinity of the interfaces. Consequently, the phase separation in the NDZs is microscopically and kinetically different from that in the inner ferrite. The nucleation and growth of G-phase in the NDZs are suppressed, and the growth of  $\alpha'$ -phase is decelerated. In contrast, the G-phase at the austenite/ferrite interfaces exhibits a delayed heterogeneous nucleation and thereafter accelerated growth. The phase-separation difference between the NDZ and the inner ferrite results in a gradient microstructure (from outer to inner) developing in each ferrite grain during the prolonged aging. The strong segregation of Ni and the high decoration of G-phase at the ferrite/austenite interface are responsible for degradation in impact toughness of the steel.

© 2017 Acta Materialia Inc. Published by Elsevier Ltd. All rights reserved.

## 1. Introduction

Duplex stainless steels (DSS), with high strengths, excellent stress-corrosion resistance and good weldability, have a broad range of engineering applications, including in nuclear power, chemical processing, desalination and transportation industries [1]. The steels during long-term service at a temperature in the range from 280° to 320 °C suffer with thermal embrittlement due to phase separation of ferrite [2]. Consequently, their mechanical properties and performances including fracture toughness [3], stress corrosion resistance [4] and fatigue properties [5,6] deteriorate. A significant degradation of the DSSs during service will pose a great risk to the safe operation of nuclear power plants. As a result, fundamental understandings about the thermally-induced microstructural evolution of the steels have drawn huge research interests.

Thermally-induced microstructural changes of duplex stainless steels with high Cr contents mainly involve the formation of Cr-rich ( $\alpha'$ ) phase and Fe-rich ( $\alpha$ ) phase [7–9], as well as G-phase in ferrite

because of phase separation [1,10,11]. M23C6 precipitation on ferrite/austenite boundaries has been observed as well [12,13]. To understand the formation of Cr-rich ( $\alpha'$ ) phase and Fe-rich ( $\alpha$ ) phase, binary Fe-Cr alloys have been extensively studied over the last 70 years [14–18]. The phase-separation behaviours of the Fe-Cr alloys are found to be highly dependent on the alloy's Cr content and aging temperature, with the  $\alpha'$ -phase in the form of isolated particles or vein-like structures depending on the spinodal line of the Fe-Cr system [19–21].

Ni, as an important alloying element of DSSs, has complicated effects on the phase separation of ferrite. Firstly, Ni addition enhances phase separation kinetics of the Fe-Cr alloys. J.E. Brown [22] reported that the addition of Ni increased the rate of spinodal decomposition by studying a series of Fe-26% Cr-(0-3-5-8)% Ni alloys upon aging in the temperature range from 300 to 450 °C. A similar effect has been observed in DSSs [2]. Secondly, Ni is responsible for the G-phase formation in the ternary Fe-Cr-Ni system. G.T. Brown and R.T. Allsop [23], for the first time, observed G-phase particles in a Fe-12Cr-4Ni alloy thermally aged at 450 °C in 1960. Thereafter, the G-phase was widely reported in the DSSs. Si, Mn and Ni are reported to induce the G-phase precipitation in the DSSs [8,24,25]. The spinodal decomposition of ferrite has been found to enhance the G-phase precipitation, because the

\* Corresponding author. School of Materials Science and Engineering, Nanjing University of Science and Technology, Nanjing, 210094, China.

E-mail address: [gang.sha@njjust.edu.cn](mailto:gang.sha@njjust.edu.cn) (G. Sha).

enrichment of the G-former elements at the  $\alpha'/\alpha$  inter-domains provides favourable conditions for the formation of the G-phase in a Mo-free DSS during aging at 350 °C [26]. Previous research has mostly focused on the microstructural change of the inner ferrite; this has greatly limited our understanding about phase separation in ferrite of the DSSs.

Ferrite/austenite interfaces in DSSs are known to be important for plastification of the neighbouring ferrite grains and crack initiation [27], and are of significance in determining the mechanical properties of the steels [28,29]. To date, little work has been done in addressing the phase separation near the ferrite/austenite phase boundaries of the DSSs. T. Hamaoka et al. [25,30] found that G-phase particles were small near the phase boundary in a DSS (designated as CF3M) aged at 400 °C for 5000 h and their number density increased with the distance from the phase boundary. There is a lack of information regarding the segregation of alloying elements and impurities as well as the precipitation at the ferrite/austenite interfaces of the DSSs during thermal aging. It is unclear if the phase separation across a ferrite grain is uniform, and how the ferrite/austenite interface affects the nucleation and growth of G-phase as well as the formation of Cr-rich ( $\alpha'$ ) phase and Fe-rich ( $\alpha$ ) phase near the interface. Comprehensive investigation of the ferrite/austenite interfaces is necessary for pinpointing the key microstructures or phases responsible for the mechanical properties and performance of the steels.

In this study, we systematically investigate the thermal decomposition of a duplex steel with an emphasis on addressing the segregation and precipitation at ferrite/austenite phase boundaries, and the non-uniformity of phase separation in a ferrite grain. To achieve this, a focused ion beam (FIB) has been employed to prepare atom-probe tip samples containing  $\delta/\gamma$  interfaces, to overcome the technical difficulties in making such samples by electro-polishing. Atom probe tomography (APT) offers a high spatial resolution and a high chemical sensitivity, it is employed to quantitatively characterise the distribution, partition and segregation of alloying elements and impurities in the steel. This research aims to comprehensively address the phase-separation mechanisms of the ferrite grain in the steel. By systematically measuring the evolutions of size, number density and chemical compositions of precipitates and phases formed in the different regions of the ferrite grain, this research will reveal the phase-separation kinetics in the different regions of the ferrite grain, and identify key microstructural features important for thermal embrittlement of the steel.

## 2. Experiments

A duplex stainless steel (designated Z3CN20-09M) with a nominal chemical composition listed in Table 1 was used in this work. The composition of the steel is similar to that used in the primary circuit pipeline of a nuclear power plant. The typical microstructure of the cast steel quenched in water after a homogenization treatment at 1100 °C for 6.5 h is shown in Fig. 1, which consists of ferrite in a dark contrast and austenite in a light grey contrast. The area fraction of the ferrite was measured to be less than 20% using Ferrite Scope (Fischer Feritscope MP30). Thermal aging of the steel was carried out at 400 °C for up to 20,000 h.

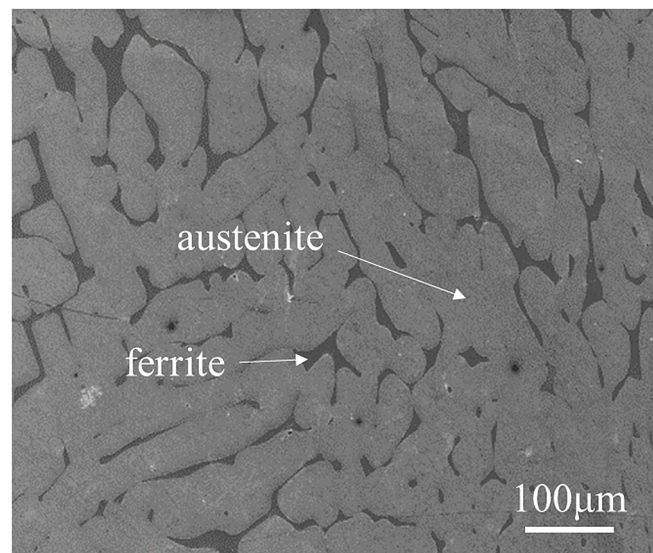


Fig. 1. A SEM micrograph of a duplex steel in as-cast condition.

Charpy V-notch impact tests at room temperature were conducted on the as-cast and thermally aged samples. Charpy specimens with a size of 10 mm × 10 mm × 55 mm with a 45° V-notch at the centre were machined according to the ISO standard 14556:2000 [31]. Since no thermal decomposition occurred in the austenite of the duplex stainless steel, nano-indentation tests were performed only on the large ferrite phases with an objective to avoid the influence of the underlying soft austenite and edge effects of grain/phase boundaries. Before nano-indentation, all finely polished specimens were slightly etched to clearly reveal ferrite and austenite regions in the microstructures. The nano-indentation measurements were performed by using an MTS Nano-Indenter DCM tester with a 20 mN load. Each hardness value reported in this work was taken from the mean of at least five nano-hardness measurements from the ferrite of each specimen.

For atom probe tomography analysis, sharp APT tip samples containing ferrite/austenite interfaces were fabricated by FIB milling in a Zeiss Auriga FIB/SEM, with sample preparation procedures as summarized in Fig. 2. The region of interest containing a ferrite/austenite interface was firstly deposited with Pt to protect it from ion-beam damage during subsequent milling. Tilt and ion milling were secondly performed to cut a wedge bar out from specimen, as shown in Fig. 2a. The lift-out wedge bar specimen was thirdly cut into individual sections after each was mounted on a pre-sharpened tip or a micro-post of a Si micro-tip array coupon, as shown in Fig. 2b. Annular milling, as shown in Fig. 2c, was finally performed to produce a sharp tip with an apex radius of <50 nm, suitable for APT analysis. With this site-specific sample preparation method, tips containing an interface inclined to their shank axes were consistently made. APT experiments were performed by using a CAMECA local electrode atom probe LEAP™ 4000X Si at a specimen temperature of 20 K, under an ultrahigh vacuum of  $2.5 \times 10^{-9}$  Pa, a pulsing UV laser with a wavelength of 355 nm and a laser energy of 40 pJ, at a pulse repetition rate of 200 kHz, and an

Table 1  
Nominal composition of the steel.

Alloy	Cr	Ni	Si	Mn	Cu	Mo	Co	C	N	S	P
wt. %	20.12	9.73	1.04	0.96	<0.10	0.14	0.098	0.033	0.044	0.0009	0.014
at. %	21.13	9.05	2.02	0.95	<0.09	0.08	0.091	0.15	0.17	0.0015	0.025

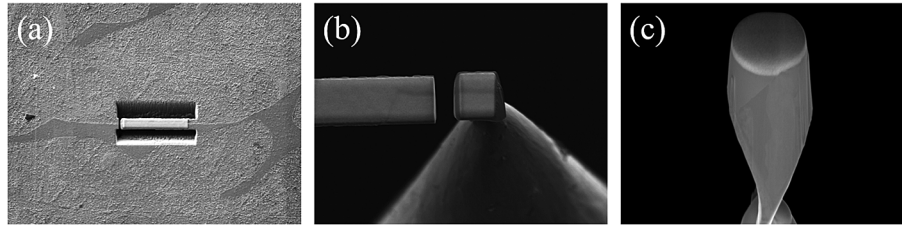


**Fig. 2.** FIB preparation of an APT specimen containing a ferrite/austenite interface. (a) SEM image of an FIB-milled wedge-shape bar containing a ferrite/austenite interface; (b) an individual cut from the wedge bar mounted on a Si post; (c) annular milled the mounted sample.

ion collection rate of 0.5% per pulse. APT data reconstruction and quantitative analysis were carried out using the CAMECA IVAS version 3.6.8 software.

### 3. Results

#### 3.1. Hardening of ferrite and embrittlement of the steel during thermal aging

Fig. 3a shows the evolution of nano-hardness of the ferrite in the steel during aging at 400 °C. The nano-hardness of ferrite in the stainless steel increased significantly with aging time. The initial nano-hardness of the ferrite in the as-cast steel was 2.9 GPa. It reached 8.5 GPa after 20,000 h aging. It is worthwhile noting that the increment in the nano-hardness of the ferrite becomes less significant after aging over 10,000 h. The evolution of impact energy of the steel with aging time is shown in Fig. 3b. The total impact energy  $W_t$ , crack initiation energy  $W_i$  and crack propagation energy  $W_p$  remarkably decreased with aging time. Before 3000 h aging, the impact energy of the steel dropped dramatically with aging time, whereas after 3000 h aging, the energy decreased slowly. The reduction of the impact energy of the steel is coincident with the increase of nano-hardness of the ferrite. To understand the microstructures of the steel samples aged at different stages, APT characterizations were performed on specimens aged for 0 h, 3000 h and 20,000 h.

#### 3.2. Distributions of solutes in the duplex steel before and after thermal aging

Fig. 4 shows atom probe analysis of an as-quench sample after a homogenization treatment at 1100 °C. The analysed volume consists of an austenite grain, a ferrite grain and their mutual phase boundary, as seen in Fig. 4a. Cr strongly partitioned into the ferrite, in contrast, Ni, Mn, Cu and C strongly partitioned into the austenite

as seen in a Cr atom map (Fig. 4a). All elements appear to be uniformly distributed inside each grain. This is further confirmed by nearest-neighbour (NN) analysis of each element in the ferrite grain, as shown in Fig. 4b. Quantitative measurements, as listed in Table 2, confirm that the concentrations of Ni, Mn and Cu in the ferrite are lower than those in the austenite, respectively. The ferrite/austenite interface of the specimen was observed with a clear enrichment of Mo, C, P and B, but a slight depletion of Fe and Cr, and insignificant enrichment of Ni, Mn, Si and Cu, as seen in 1D concentration profiles across the interface (Fig. 4c). This indicates that different elements segregate differently at the ferrite/austenite interface. Solute excess values measured at the ferrite/austenite interface of the as-cast steel are listed in Table 3. Mo and B are the two strongest segregants at the interface of the steel, with solute excess values of 3.34 and 4.49 atoms/nm<sup>2</sup>, respectively. The excesses of C and P at the interface are 1.67 and 1.33 atoms/nm<sup>2</sup>, respectively, higher than those of Mn, Si and Cu.

Fig. 5 shows atom probe examination of a specimen aged for 3000 h at 400 °C. The analysed volume consists of a ferrite grain, an austenite grain and a ferrite/austenite interface. All elements appear to be homogeneous inside both the ferrite and the austenite grains by a visual examination of these atom maps (Fig. 5a). However, NN analyses of the atom pairs of alloying elements (Fig. 5b) clearly demonstrated that Cr, Ni, Si and Mn atoms in the ferrite slightly developed non-random distributions, as corresponding experimental curves were parting to the left of the reference curves (in red) with these elements in random distributions. Careful examinations of a small selected volume from the ferrite, as shown in Fig. 5d, confirmed that interconnected Cr-rich domains ( $\alpha'$ -phase) and Cr-lean domains ( $\alpha$ -phase) formed and equi-axed Ni-rich features (G-phase) precipitated as well. The compositions of the ferrite grain,  $\alpha'$ -phase and matrix ( $\alpha$ -phase) in the sample are listed in Table 2, which were measured from 1D concentration profiles (not shown here) across the analysed volumes, with Cr peaks and troughs corresponding to the centres of the  $\alpha'$ -phase domains, and

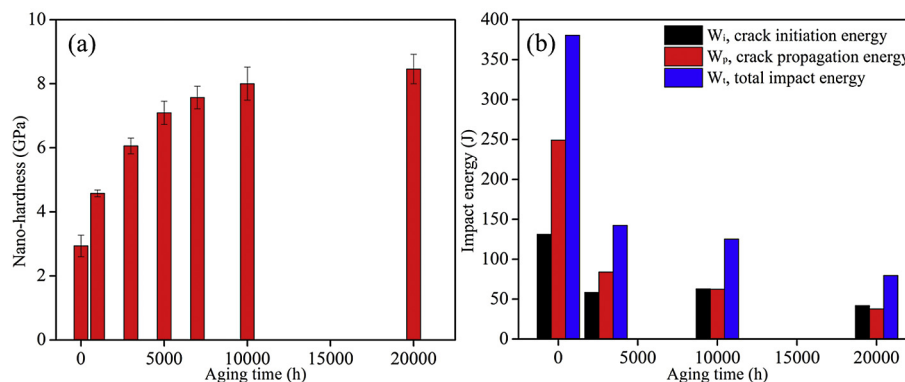


**Fig. 3.** The evolution of nano-hardness of the ferrite (a) and the evolution of impact energy of the steel (b) during thermally aging at 400 °C.

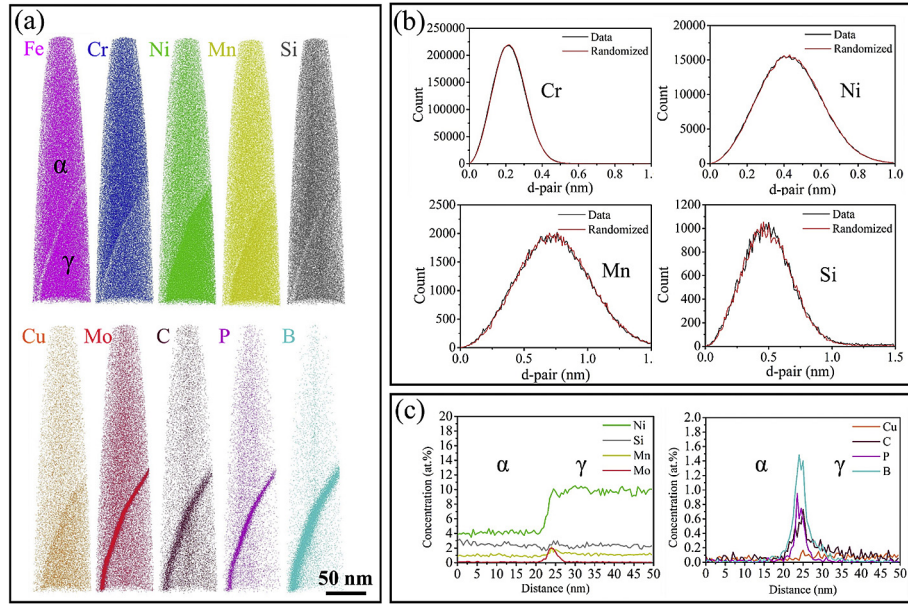


**Fig. 4.** APT characterizations of the steel in an as-cast condition. (a) Atom maps of a reconstructed volume from a data set of the as-cast steel, with ferrite in the upper part and austenite in the lower part; (b) Nearest-neighbour analyses of elements in ferrite of the as-cast steel; (c) 1D concentration profiles across the ferrite/austenite interface in the analysed volume.

**Table 2**

Compositions (at.%) of phases in the steel aged for 0 h, 3000 h and 20,000 h at 400 °C, measured by APT. Analysis regions contain ferrite, austenite,  $\alpha'$  phase and the matrix ( $\alpha$ -phase).

Aging time		Fe	Cr	Ni	Si	Mn	Cu	Mo
0 h	ferrite bulk	61.70 ± 0.021	30.34 ± 0.014	4.13 ± 0.005	2.55 ± 0.004	0.88 ± 0.002	0.03 ± 0.00	0.09 ± 0.00
	austenite bulk	66.79 ± 0.05	20.12 ± 0.03	9.52 ± 0.02	1.96 ± 0.01	1.10 ± 0.01	0.07 ± 0.00	0.07 ± 0.00
3000 h	ferrite bulk	61.93 ± 0.02	29.73 ± 0.02	4.32 ± 0.01	2.62 ± 0.01	0.93 ± 0.00	0.04 ± 0.00	0.10 ± 0.001
	austenite bulk	66.67 ± 0.03	20.41 ± 0.02	9.58 ± 0.01	1.94 ± 0.01	1.20 ± 0.004	0.07 ± 0.001	0.05 ± 0.001
	$\alpha'$ -phase	41.67 ± 0.03	50.60 ± 0.03	2.94 ± 0.01	3.09 ± 0.01	1.14 ± 0.01	0.06 ± 0.001	0.15 ± 0.002
20,000 h	$\alpha$ -phase	73.31 ± 0.07	17.88 ± 0.03	5.08 ± 0.02	2.34 ± 0.01	0.78 ± 0.01	0.08 ± 0.002	0.10 ± 0.002
	ferrite bulk	61.68 ± 0.02	29.61 ± 0.01	4.22 ± 0.01	2.53 ± 0.004	0.89 ± 0.002	0.03 ± 0.001	0.11 ± 0.001
	austenite bulk	66.76 ± 0.04	20.28 ± 0.02	9.46 ± 0.01	1.94 ± 0.01	1.07 ± 0.01	0.06 ± 0.001	0.03 ± 0.001
	$\alpha'$ -phase	29.70 ± 0.02	64.19 ± 0.03	1.74 ± 0.01	2.81 ± 0.01	1.00 ± 0.004	0.04 ± 0.001	0.22 ± 0.002
	$\alpha$ -phase	79.59 ± 0.03	10.37 ± 0.01	6.23 ± 0.01	2.30 ± 0.01	0.86 ± 0.003	0.06 ± 0.001	0.11 ± 0.001

**Table 3**

Solute excesses at ferrite/austenite phase boundaries (atoms/nm<sup>2</sup>) aged at 400 °C for different time.

Aging time	Ni	Si	Mn	Cu	Mo	B	C	P
0 h	—	0.88 ± 0.05	0.97 ± 0.06	0.04 ± 0.01	3.34 ± 0.10	4.49 ± 0.12	1.67 ± 0.07	1.33 ± 0.07
3000 h	16.11 ± 0.23	1.96 ± 0.08	1.79 ± 0.08	0.11 ± 0.02	2.36 ± 0.09	3.18 ± 0.10	1.95 ± 0.08	0.62 ± 0.04
20,000 h	43.56 ± 0.37	8.47 ± 0.16	7.92 ± 0.16	0.33 ± 0.03	2.21 ± 0.08	1.25 ± 0.06	2.17 ± 0.08	1.03 ± 0.06

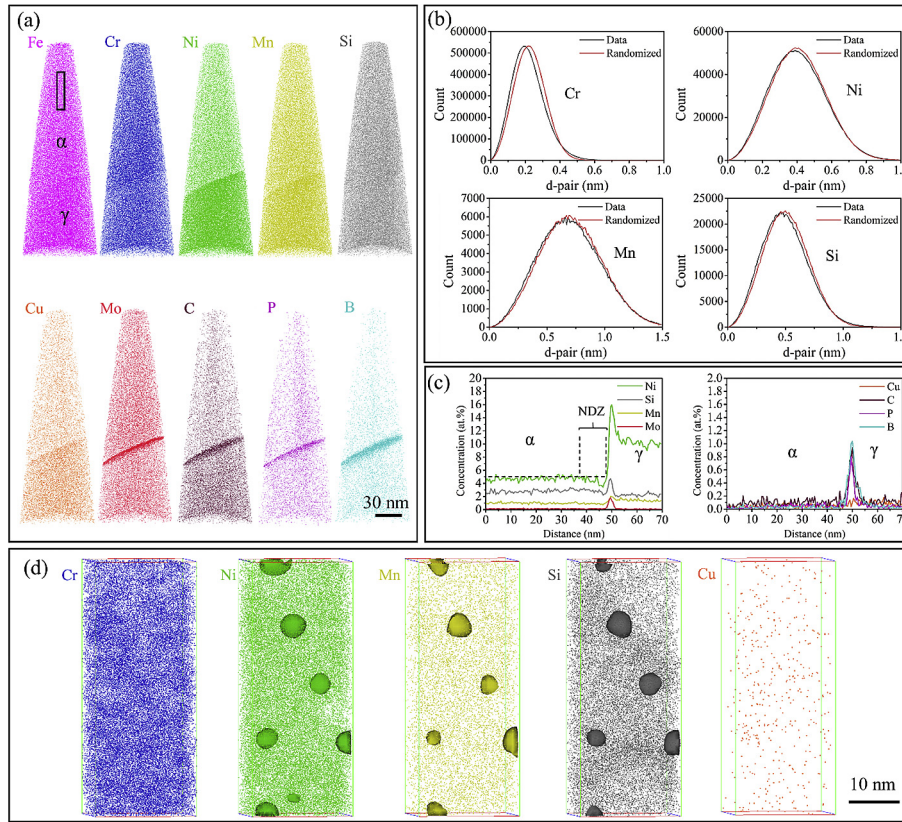
the centres of  $\alpha$ -phase domains, respectively. The mean concentrations of  $\alpha'$ -phase and the matrix ( $\alpha$ -phase) are the averages of values measured at the  $\alpha'$ -phase centres, and the matrix ( $\alpha$ -phase) centres, respectively. Si, Mn and Mo enrich in  $\alpha'$ -phase rather than in the  $\alpha$ -phase. In contrast, Ni and Fe are lean in the  $\alpha'$ -phase.

After 3000 h aging, in addition to Mo, C, P and B, the segregation of Mn and Si at the ferrite/austenite interface became evident, as seen in the 1D concentration profiles obtained across the interface (Fig. 5c). Most strikingly, Ni developed strong segregation at the interface, indicating that aging induced the segregation of Ni at the interface. Solute excesses of these elements measured at the interface are listed in Table 3. The solute excess of Ni at the interface became 16.1 atom/nm<sup>2</sup>, the highest one over the rest of other elements Si, Mn, Mo, B and C etc. It is worth noting here that a Ni depletion zone (NDZ) of approximately 9 nm in width was

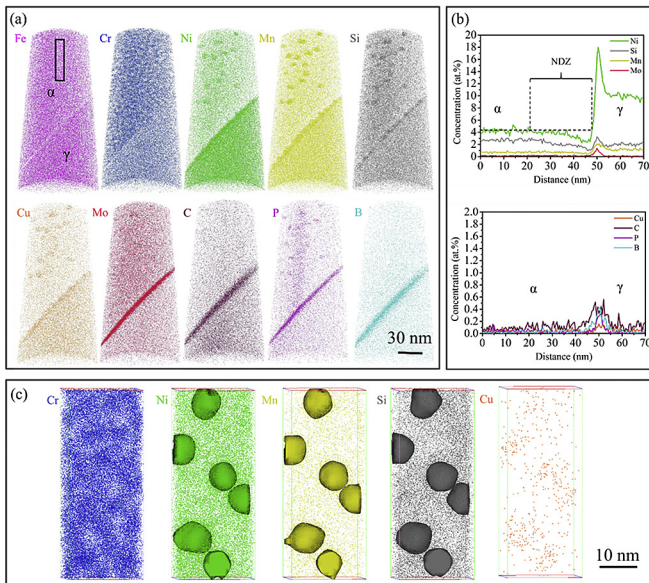
observed to the left of the  $\alpha/\gamma$  interface, as seen in Fig. 5c.

Fig. 6 shows APT examination of a sample aged for 20,000 h at 400 °C. The analysed volume consists of a ferrite grain, an austenite grain and a ferrite/austenite interface (Fig. 6a). All elements in the austenite grain remained in a random distribution. A further development of the phase separation of ferrite in the steel is evidenced. The Cr-rich domains ( $\alpha'$ -phase), and Cr-lean domains ( $\alpha$ -phase) were further developed, as clearly seen in Fig. 6a and c. Meanwhile, Ni-rich features (G-phase) in the ferrite grain reached an average size of ~10 nm, and were enriched with Mn, Si, Cu, Mo and P, as seen in corresponding atoms maps (Fig. 6a).

After 20,000 h aging, the segregation at the ferrite/austenite interface developed further (Fig. 6a). In particular, the segregation of Ni, Mn, Si and Cu at the interface became much stronger than aged for 3000 h, as seen in Table 3 and Fig. 6b. The NDZ in the ferrite



**Fig. 5.** APT characterizations of the steel aged at 400 °C for 3000 h. (a) Atom maps of an analysed volume with ferrite in the upper part and austenite in the lower part; (b) Nearest-neighbour count distributions of elements in the ferrite; (c) 1D concentration profiles across the ferrite/austenite interface in the volume; (d) 3D atoms distributions in a small volume of  $50 \times 20 \times 20 \text{ nm}^3$  obtained from the ferrite region, with Ni isosurfaces (in green) at 25 at.%, Mn isosurface (in yellow) at 4 at.%, Si isosurfaces (in grey) at 7 at.%. (For interpretation of the references to colour in this figure legend, the reader is referred to the web version of this article.)



**Fig. 6.** APT characterizations of the steel aged at 400 °C for 20,000 h. (a) Atom maps of the analysed volume with ferrite in the upper part and the austenite in the lower part; (b) 1D concentration profiles across ferrite/austenite interfaces; (c) 3D atoms distributions of a small volume of  $50 \times 20 \times 20 \text{ nm}^3$  obtained from the ferrite region, Ni isosurfaces (in green) at 25 at.%, Mn isosurfaces (in yellow) at 4 at.%, and Si isosurfaces (in grey) at 7 at.%. (For interpretation of the references to colour in this figure legend, the reader is referred to the web version of this article.)

side near the  $\alpha/\gamma$  interface became about 30 nm in width (Fig. 6b), and was free of the G-phase precipitates, as seen in the Ni map (Fig. 6a). Careful examination revealed that the  $\alpha/\gamma$  interface was highly decorated with G-phase particles (Ni, Mn, Si and Cu maps in Fig. 6a). To our knowledge, this is the first recorded observation of the heterogeneous nucleation of G-phase at the  $\alpha/\gamma$  interface and the formation of the NDZ in the ferrite near the  $\alpha/\gamma$  interface. The G-phase particles at the ferrite/austenite interface have chemical compositions slightly different from those in the inner ferrite of the steel aged for 20,000 h, as shown in Table 4. In particular, their Ni, Si, Mn and Cu levels are lower than those formed in the inner ferrite, while the Mo concentration is higher. The higher Mo concentration of the G-phase at the interface than that in the inner ferrite is likely due to the strong segregation of Mo at the interface, as seen in Fig. 6b.

### 3.3. Phase separation of inner ferrite in the duplex stainless steel during aging at 400 °C

#### 3.3.1. Evolution of $\alpha'$ -phase in chemistry and size

The compositions of  $\alpha'$ -phase and the matrix ( $\alpha$ -phase) in the inner ferrite grains evolved significantly with aging time as listed in Table 2. In particular, the Cr concentration difference ( $\Delta C_{\text{Cr}}$ ) between  $\alpha'$ -phase and  $\alpha$ -phase rose significantly, and  $\Delta C_{\text{Mo}}$  only increased slightly, but  $\Delta C_{\text{Fe}}$  and  $\Delta C_{\text{Ni}}$  decreased with increasing aging time. This is consistent with a spinodal decomposition of ferrite occurring in the steel during aging at 400 °C. Interestingly, after 20,000 h aging,  $\Delta C_{\text{Si}}$  and  $\Delta C_{\text{Mn}}$  all decreased in contrast to the trend observed for  $\Delta C_{\text{Cr}}$ .

**Table 4**

Compositions (at. %) of the G-phase precipitates in ferrite and on the ferrite/austenite interfaces after 20,000 h aging at 400 °C.

	Fe	Cr	Ni	Si	Mn	Cu	Mo
G-phase at phase boundary	14.32 ± 0.14	5.68 ± 0.09	45.40 ± 0.25	19.22 ± 0.17	11.84 ± 0.13	0.42 ± 0.02	1.93 ± 0.05
G-phase in the inner ferrite	5.48 ± 0.03	2.43 ± 0.02	51.45 ± 0.09	21.44 ± 0.06	17.11 ± 0.05	0.55 ± 0.01	0.84 ± 0.01

To better evaluate the size evolution of the  $\alpha'$ -phase and the  $\alpha$ -phase domains during the spinodal decomposition in the steel, the wavelength ( $\lambda$ ) of composition fluctuation in the ferrite was deduced based on autocorrelation function [32–35], by using the autocorrelation efficient plots (Fig. 7), extracted from 1D Cr concentration profiles measured by a small cylinder across each analysed volume (Fig. 7a and b). The measurements were performed in a direction parallel to the shank axis of each analysed volume. It is worth noting that similar measurement results are obtained along a direction parallel to the austenite/ferrite interface as seen in discussion section. The parameter  $k_1$  is the smallest mean distance between Cr peaks and their 1st nearest neighbour Cr peaks, and  $k_2$  is the second mean distance between Cr peaks and their second nearest neighbours, and so on. We define the mean wavelength as the average of values  $k_i/i$ ,  $i = 1-5$ . The results show that the mean wavelength increases from 4.58 nm to 6.77 nm with increasing aging time from 3000 to 20,000 h. In summary, the spinodal decomposition of ferrite in the steel was associated with incremental increases in the composition differences between  $\alpha'$ -phase and  $\alpha$ -phase in Cr, Fe and Ni as well as incremental increases in the wavelength of these spinodal phases (i.e. the growth of the  $\alpha'$ -phase) with increasing aging time from 3000 to 20,000 h. Si, Mn and Mo concentrations of the  $\alpha'$ -phase and  $\alpha$ -phase exhibited little changes with increasing aging time, indicating their weak partitioning between the two phases.

**3.3.2. Evolution of the G-phase precipitates in size and chemistry**

Ni-rich G-phase has been reported to form in duplex stainless steels by diffraction and composition analysis using transmission

electron microscopy [36]. Our APT results reveal that the Ni-rich G-phase precipitates appear in the Cr-lean domains and their average size increases from 5 nm to 10 nm with an increase in aging time from 3000 to 20,000 h (Figs. 5d and 6c). The G-phase is strongly enriched with Si and Mn, and weakly with Cu after 3000 h aging. After 20,000 h aging, the partitioning of Cu, and Mo into the G-phase became further enhanced, as seen in Fig. 6c. The compositions of G-phase precipitates vs their sizes and aging time are shown in Fig. 8a. Small G-phase precipitates (less than 5 nm in size) in the sample aged for 3000 h were measured containing Ni, Si and Mn with a Ni/Si ratio close to 2.57, but a high Ni/Mn ratio of 4.64 and significant amounts of Fe and Cr. As their sizes increased, the Ni/Si ratios became close to 2.26, Ni/Mn ratio was close to 2.85. Their Fe and Cr contents dropped significantly among precipitates

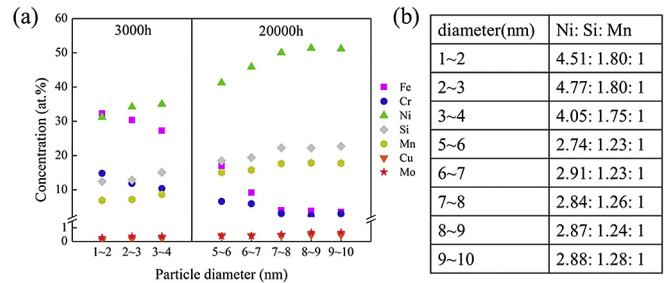


**Fig. 8.** Compositions (a) and Ni:Si:Mn ratios (b) of the G-phase precipitates as a function of the precipitate size in ferrite of the steel aged for different lengths of time. Small precipitates less than 5 nm in diameters are in the steel aged for 3000 h aging, and large precipitates are in the steel aged for 20,000 h.

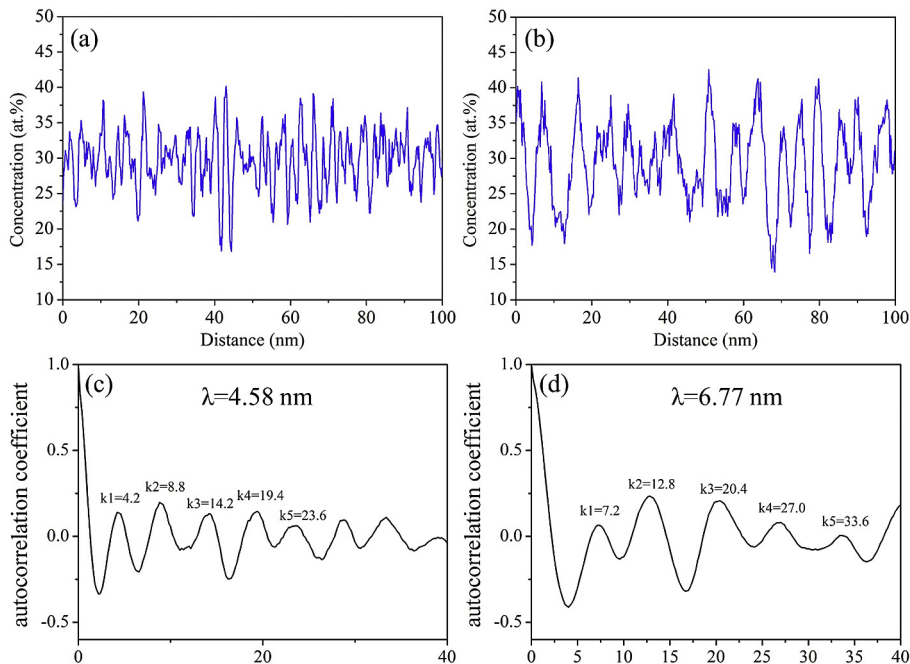


**Fig. 7.** 1-dimensional Cr concentration profiles (a, b) and corresponding autocorrelation coefficient profiles (c, d) of Cr concentration fluctuations measured from the inner ferrite of the steel aged at 400 °C. (a, c) aged for 3000 h, and (b, d) aged for 20,000 h.

with sizes less than 7 nm, and became less than 1 at. % while their sizes are larger than 7 nm. The number density of G-phase precipitates decreased from  $3.79 \pm 0.004 \times 10^{22}/\text{m}^3$  to  $0.89 \pm 0.003 \times 10^{22}/\text{m}^3$  during aging between 3000 and 20,000 h, confirming that G-phase passed its nucleation stage and was in the growth regime.

#### 4. Discussion

Thermal aging of the steel at 400 °C not only incurred the phase separation of the inner ferrite, but also induced the segregation of Ni and Si at the ferrite/austenite interface and the formation of a Ni depletion zone (NDZ) in the ferrite in the vicinity of the ferrite/austenite interface. To gain a full picture of phase separation in ferrite of the steel, it is important to know how the phase separation occur in the NDZ of ferrite as well as segregation at the austenite/ferrite interface.

##### 4.1. Segregation at the austenite/ferrite interface and formation of NDZ

Segregation at the austenite/ferrite interfaces of DSSs has seldom been systematically addressed in literature. Unlike at  $\alpha'/\alpha$  interfaces, the austenite/ferrite interface developed clear segregation of Mo, P, B and C impurities in the as-cast DSS quenched after a homogenization treatment at 1100 °C (Fig. 4c), and formed small carbon-rich features (in dark brown) thereafter during aging (Fig. 9). Si, Mn and Cu in the as-cast steel initially had insignificant segregation at the interface with solute excesses less than 1 atom/ $\text{nm}^2$  (see Table 3), and Ni showed no segregation at the interface. However, after 3000 h and 20,000 h aging, Ni segregated strongly at the interface, with the peak concentrations of ~16 at.% and 18 at.% Ni (Figs. 5c and 6b), respectively, confirming that aging-induced segregation of Ni at the interface occurred. The formation of a NDZ only in the ferrite in the vicinity of the interface (Figs. 4c, 5c and 6b) indicates that the segregation of Ni at the  $\alpha/\gamma$  interface is mainly due to the diffusion of Ni from the ferrite, rather than from austenite. Interestingly, the segregation of G-phase former elements (Si, Mn and Cu) at the interface became stronger after aging, with excess values twice of those in the as-cast steel. In contrast, the segregation of C, and P did not change significantly, but the segregation of B and Mo decreased after the aging (Table 3). This is probably due to the growth of carbon-rich features (likely carbides) by consumption of B and Mo atoms at the interface (Fig. 9). After further aging to 20,000 h, the excesses of Ni, Si, Mn and Cu at the interface are about 4 times those aged for 3000 h. This is consistent

with the NDZ's width of about 30 nm, which is close to 3.3 times of that found in the sample age for 3000 h, as evidenced in Figs. 5c and 6b. It is noted here that 1-D concentration profiles in Figs. 5c and 6b and interfacial excess values in Table 3 exclude any G-phase precipitates at the austenite/ferrite interface.

It is known that austenite phase will dissolve more Ni at isothermal aging temperature than at the homogenization temperature of 1100 °C. This might lead to the diffusion of Ni from the ferrite to the austenite during the isothermal aging and the accumulation of Ni at the austenite/ferrite interface if Ni diffusion in the austenite is too slow. In this case, it is expected that the Ni content at the interface will not exceed a Ni content in the austenite which is equilibrium with the ferrite. Since the Ni content in the austenite in the vicinity of the austenite/ferrite interface does not show any clear increase, but Ni peak content at the interface continuously increases over 20,000 h aging at 400 °C (see in Figs. 4–6, as well as Table 3), it is concluded here that the observed increasing segregation of Ni to the austenite/ferrite interface is unlikely driven by the austenite-ferrite phase equilibrium at this isothermal aging temperature. The interface segregation is more likely driven by a lowering of the interfacial free energy, i.e. a true thermodynamic Gibbsian interfacial excess.

##### 4.2. Phase separation in the NDZ of ferrite

The phase separation in the NDZ is thermodynamically and kinetically different from that in the inner ferrite. Thermodynamically, the G-phase formation is suppressed; and kinetically spinodal decomposition to form  $\alpha'$ -phase and  $\alpha$ -phase is slowed-down in the NDZ.

##### 4.2.1. Thermodynamics: suppressed formation of G-phase precipitates

The microstructure of ferrite near the ferrite/austenite interface after the phase separation at 400 °C for 20,000 h can be clearly seen by examining a thin slice of a reconstructed volume, with  $\alpha'$ -phase domains highlighted by isosurfaces at 25 at.% Cr (blue) and G-phase precipitates highlighted by isosurfaces (green) at 32 at. % Ni, as shown in Fig. 10. No G-phase is visible in the NDZ within about 30 nm to the left of the austenite/ferrite interface. This indicates that nucleation and growth of G-phase precipitates are fully suppressed in the NDZ. A similar phenomenon was also observed in the NDZ after 3000 h aging (Fig. 11), although the NDZ is much narrower and ~9 nm in width. Interestingly, small G-phase precipitates of 5 nm in size were present just outside of the NDZ (about 9 nm away from the interface), as marked by two arrows in Fig. 11. These

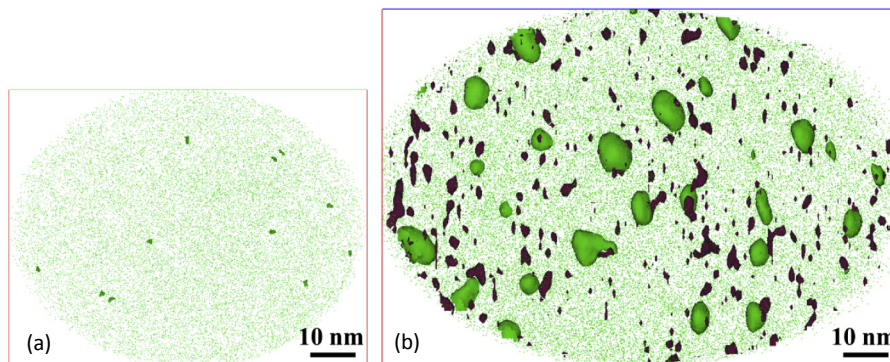
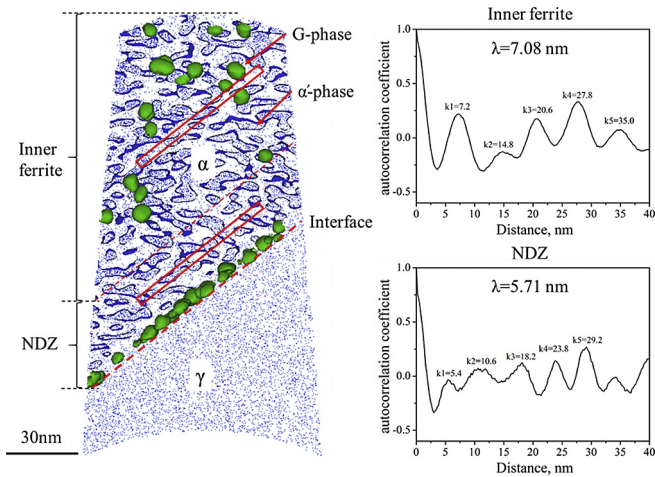
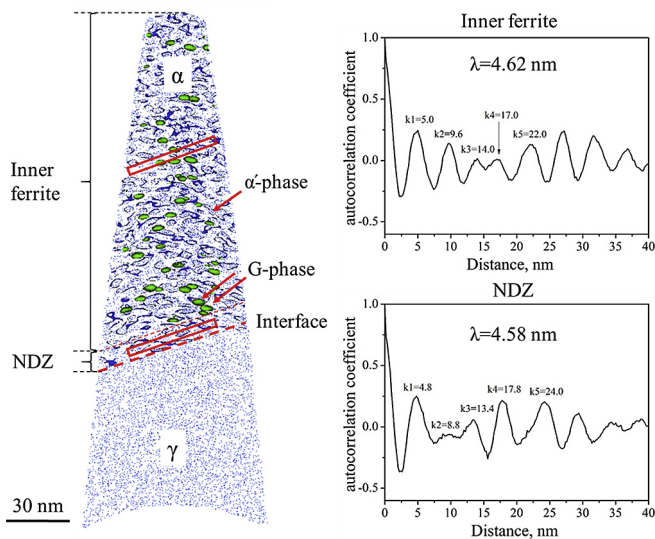


Fig. 9. Ferrite/austenite interfaces decorated with Ni-rich clusters/G-phase precipitates (viewed along the interface normal) in the steel samples aged at 400 °C for (a) 3000 h, and (b) 20,000 h, with Ni atoms in green, C atoms in dark brown. Ni iso-surfaces at 25 at.%, C iso-surfaces at 1 at.%. (For interpretation of the references to colour in this figure legend, the reader is referred to the web version of this article.)



**Fig. 10.** Phase separation of ferrite consisting of an inner ferrite region and a NDZ next to the ferrite/austenite interface, distributed with  $\alpha'$ -phase (in blue),  $\alpha$ -phase (light blue) and G-phase particles (green) in the steel aged at 400 °C for 20,000 h (left), and autocorrelation coefficient profiles of Cr concentration fluctuation measured from the two marked regions in the inner ferrite and the NDZ, respectively (right). Cr isoconcentration is 32 at.%, Ni isoconcentration is 25 at.%. The image is a thin slice (1 nm thick) taken from the reconstructed volume of an APT dataset in Fig. 6. (For interpretation of the references to colour in this figure legend, the reader is referred to the web version of this article.)



**Fig. 11.** Phase separation of ferrite with  $\alpha'$ -phase (in blue),  $\alpha$ -phase (in light blue) and G-phase (green) distributing in the inner ferrite and the NDZ in the vicinity of a ferrite/austenite interface of the steel aged at 400 °C for 3000 h (left), and autocorrelation coefficient profile of Cr concentration fluctuation in the inner ferrite and the NDZ (right). Cr isoconcentration is 32 at.%, Ni isoconcentration is 25 at.%. The image is a thin slice (1 nm thick) partially taken from the reconstructed volume of an APT dataset shown in Fig. 5. (For interpretation of the references to colour in this figure legend, the reader is referred to the web version of this article.)

small G-phase precipitates within 30 nm from the interface in the ferrite aged for 3000 h extinguished in the 30 nm thick NDZ after 20,000 h aging (Fig. 10), i.e. the dissolution of the pre-existing G-phase precipitates occurs with the advance of NDZs during aging. This clearly indicates that G-phase thermodynamically is unstable in the NDZs of the steel.

The G-phase formation is reported to be sensitive to the Ni contents of DSSs [1]. Alloy 2003 with 3.7 wt.% Ni, unlike alloy 2205 with 5.69 wt.% Ni, has no G-phase precipitation during aging at

427 °C. In our DSS, Ni content of the ferrite was measured to be in the range of 4.13–4.32 at.%, as seen in Table 2. Ni content in the NDZ of the alloy aged for 20,000 h, as seen in the 1D concentration profile (Fig. 6b), decrease gradually with decreasing distance from the austenite/ferrite interface. Within 20 nm from the interface, Ni content drops below 4 at.% and to the minimum value of 2.5 at.% Ni finally. Such a low Ni content may explain the suppression of G-phase formation in the region. However, it does not work for the NDZ between 20 and 30 nm from the interface because the Ni content is above 4 at.% Ni. The dissolution of G-phase precipitates in the region after 20,000 h aging must be due to being in the diffusion affected zone of the interface segregation and precipitation. It is likely that the segregation of Ni and Si at the austenite/ferrite interface drops the system Gibbs energy much greater than the growth of G-phase in the NDZ. As a result, the pre-existing small G-phase precipitates within 30 nm from the interface observed after 3000 h aging (see Fig. 11) dissolved completely after 20,000 h aging.

#### 4.2.2. Kinetics: slowed-down formation of $\alpha'$ -phase

There is a spinodal decomposition in the NDZ as seen in Figs. 10 and 11. After 20,000 h aging, the  $\alpha'$ -phase in the NDZ was measured with a Cr concentration of 61.15 at.%, lower than 64.59 at.% of the  $\alpha'$ -phase in the inner ferrite (Table 5). In addition, the wavelength of the Cr concentration fluctuation in the NDZ is 5.71 nm, larger than 7.08 nm of that in the inner ferrite (Fig. 10). This clearly indicates that the spinodal decomposition in the NDZ was less developed than that in the inner ferrite after 20,000 h aging. To evaluate the slowdown effect of the spinodal decomposition in the NDZ, the wavelength change of spinodal decomposition was measured to be 1.13 nm in the NDZ, less than half of the value (2.46 nm) in the inner ferrite during aging between 3000 and 20,000 h. Therefore, it is safe to conclude that the growth of  $\alpha'$ -phase in the NDZ slows down considerably in comparison with that in the inner ferrite during the prolonged aging. Given that the size evolution of  $\alpha'$ -phase should follow  $r(t) = k_r t^n$ , where  $k_r$  is a rate constant and  $n$  is the time exponent [37], this slowed-down growth might be correlated to a decrease of time exponent in the NDZ. The austenite/ferrite interfaces in the steel might serve as effective vacancy sinks, similar to grain boundaries in Al alloys [38]. As a result, the vacancy concentration and related diffusion coefficients in the NDZ would drop significantly. This would kinetically slow-down the decomposition in the NDZ. It has been reported that Ni has an acceleration effect on the spinodal decomposition of  $\alpha$ - $\alpha'$  phases [2]. The low Ni content in the NDZ may be another factor responsible for the slow  $\alpha'$ -phase formation.

#### 4.3. Nucleation and growth of G-phase on the ferrite/austenite interface

Small Ni-rich clusters (precursor of G-Phase) were observed on the interface (Fig. 9a) after 3000 h aging. This indicates that the interface served as a favourable site for heterogeneous nucleation of G-phase. It is a surprise that the Ni-rich clusters at the interface are only approximately 1 nm in size, much smaller than those (~5 nm) in the inner ferrite (Figs. 5d and 6c). This suggests that the nucleation of G-phase at the interface requires a longer incubation period than that in the inner ferrite. Ni showed a very strong segregation at the ferrite/austenite interface with a solute excess of 16.11 atom/nm<sup>2</sup> after 3000 h aging. This excess value is very high because the interface would be fully occupied by Ni if the excess Ni atoms only occupied a single atomic plane (interface). The interface must have a very high Ni solubility, and hence causes the delayed nucleation of the G-phase at the interface. The average composition of these small Ni-rich clusters is 27.6 at.% Ni, 5.1 at.% Si, 3.1 at.% Mn, 0.16 at.% Cu and 1.6 at.% Mo, slightly different from those formed in

**Table 5**  
Compositions of  $\alpha'$ -phase (at. %) in the inner ferrite and a NDZ of the steel aged for 20,000 h.

		Fe	Cr	Ni	Si	Mn	Cu	Mo
$\alpha'$ -phase	Inner ferrite	32.88 ± 0.04	61.15 ± 0.07	1.78 ± 0.01	2.67 ± 0.01	0.80 ± 0.01	0.02 ± 0.001	0.25 ± 0.003
	NDZ	29.23 ± 0.03	64.59 ± 0.03	1.79 ± 0.01	2.87 ± 0.01	0.99 ± 0.004	0.04 ± 0.0005	0.18 ± 0.002

the inner ferrite region. In particular, their Mo concentrations are higher, but Ni, Si and Mn concentrations are slightly lower.

After 20,000 h aging, G-phase particles at the interface grew to sizes close to 10 nm in diameter (Fig. 9b), similar to those in the inner ferrite region (Fig. 6b). The size change of the G-phase precipitates on the interface (from 1 nm to 10 nm) is much larger than that (from 5 nm to 10 nm) in the inner ferrite, indicating that the G-phase precipitates on the interface grow at a fast rate, twice of that in the inner ferrite. The fast diffusion of Ni along the interface may facilitate the fast growth of the G-phase precipitates.

#### 4.4. Correlation between microstructure and mechanical properties of the steel

This research, for the first time, unveils that the phase separation of a ferrite grain in the DSS is non-uniform in nature with the strong segregation of Ni at the austenite/ferrite interface and the formation of NDZs during a long-term thermal aging. In comparison with the thicknesses of ferrite grains (10–20  $\mu\text{m}$ , Fig. 1), the NDZs with thicknesses < about 30 nm should have little effect on the nano-hardness of the ferrite. Therefore, the formation of  $\alpha'$ -phase and the precipitation of G-phase in the inner ferrite during aging (Figs. 5a and 6a) are responsible for the observed hardening effect of the steel (Fig. 3a). It is known that cracks initiate at the austenite/ferrite interfaces of the DSSs [39], and G-phase precipitation in DSSs is harmful for the impact toughness of the DSSs [1]. Since long-term aging induces the strong segregation of Ni and the decoration of the G-phase precipitates on the interfaces, they are likely the key microstructures responsible for the degraded impact toughness of the steel. This implies that if the G-phase precipitation on the interfaces and Ni segregation were restrained properly, the fracture toughness of the DSS could be enhanced effectively. The less-developed phase separation in the NDZ should produce a weak hardening effect, and should make each ferrite grain possess a soft shell. This gradient microstructure from outer to inner of the ferrite grain could be important for crack propagation in the steel, if it were engineered properly. More research in this area may open new opportunities in developing alloys with enhanced impact toughness.

## 5. Conclusions

Thermal aging at 400 °C had complicated effects on the microstructure and mechanical properties of a duplex stainless steel. Detailed APT investigations reached the following conclusions:

- 1 The phase separation across individual ferrite grains are not uniform microscopically and kinetically in the duplex stainless steel during aging at 400 °C. The thermal aging induced the strong segregation of Ni from ferrite towards austenite/ferrite interfaces and the formation of Ni depletion zones (NDZs) with a width of about 30 nm in the vicinity of the interface after 20,000 h aging.
- 2 Microscopically, the phase separation in the inner ferrite consists of the formation of  $\alpha'$ -phase and  $\alpha$ -phase by a spinodal decomposition, as well as precipitation of G-phase. In contrast,

the phase separation in the NDZ only involved the formation of  $\alpha'$ -phase and  $\alpha$ -phase, with the suppression of G-phase's nucleation and growth.

- 3 Kinetically, the formation of  $\alpha'$ -phase in the NDZs was slowed down considerably in comparison with that in the inner ferrite during prolonged aging. This is likely due to the low Ni content in the NDZs and slow diffusion of Cr and Fe correlated with reduced vacancy concentrations in the NDZ.
- 4 The ferrite/austenite interface is a favourable site for heterogeneous nucleation of the G-phase in the steel. The G-phase on the interface showed delayed nucleation but accelerated growth during the prolonged aging. The longer incubation time for G-phase nucleation on the interface than in the inner ferrite is likely due to the high solubility of Ni at the austenite/ferrite interface.
- 5 Among all alloying elements and impurities including Si, Mn, Cu, Mo, B, C, P and B in the steel, Ni is the strongest segregant at the interface with solute excesses above 16 atom/nm<sup>2</sup> after 3000 h aging, and 43 atom/nm<sup>2</sup> after 20,000 h.
- 6 The formation of  $\alpha'$ -phase and  $\alpha$ -phase and precipitation of G-phase in the inner ferrite is correlated with the hardening effect of ferrite of the steel during the thermal aging, and the formation of G-phase on the austenite/ferrite interface and the segregation of Ni at the interface are correlated with the degradation in impact toughness of the steel. The slow formation of  $\alpha'$ -phase in the NDZ leads to a ferrite grain developing a soft shell after prolonged aging. Engineering such gradient microstructure of ferrite could be important in controlling fracture behaviour of the steel.

## Acknowledgements

The authors acknowledge the facilities as well as scientific and technical assistance of the Materials Characterization Facility of Nanjing University of Science and Technology. YHZ would like to acknowledge support by National Natural Science Foundation of China (51225102 and 2012CB932203), the 8th Liu Da Ren Cai Gao Feng (B932203) from Jiangsu Province, China, and the Jiangsu Key Laboratory of Advanced Nanomaterials and Technologies. LSL would like to thank the National Natural Science Foundation of China for its financial support (51601013).

## References

- [1] J.D. Tucker, M.K. Miller, G.A. Young, Assessment of thermal embrittlement in duplex stainless steels 2003 and 2205 for nuclear power applications, *Acta Mater.* 87 (2015) 15–24.
- [2] J. Zhou, J. Odqvist, M. Thuvander, S. Hertzman, P. Hedström, Concurrent phase separation and clustering in the ferrite phase during low temperature stress aging of duplex stainless steels weldments, *Acta Mater.* 06 (2012) 5818–5827.
- [3] T. Yamada, S. Okano, H. Kuwano, Mechanical property and microstructural change by thermal aging of SCS14A cast duplex stainless steel, *J. Nucl. Mater.* 350 (2006) 47–55.
- [4] F. Iacoviello, F. Casari, S. Gialanella, Effect of 475°C embrittlement on duplex steels localized corrosion resistance, *Corros. Sci.* 47 (2005) 909–922.
- [5] V. Calonne, A.F. Gourgues, A. Pineau, Fatigue crack propagation in cast duplex stainless steels: thermal aging and microstructural effects, *Fatigue Fract. Eng. Mater. Struct.* 27 (2004) 31–43.
- [6] J.B. Vogt, K. Massol, J. Foct, Role of the microstructure on fatigue properties of 475°C aged duplex stainless steels, *Int. J. Fatigue* 24 (2002) 627–633.
- [7] R.N. Gunn, *Duplex Stainless Steels, Microstructure, Properties and Applications*, Woodhead Publishing, Cambridge, 1997.

- [8] F. Danoix, P. Auger, Atom probe studies of the Fe-Cr and stainless steels aged at intermediate temperature: a review, *Mater. Charact.* 44 (2000) 177–201.
- [9] M.H. Mathon, Y. de Carlan, G. Geoffroy, X. Averty, A. Alamo, C.H. de Novion, A SANS investigation of the irradiation-enhanced  $\alpha$ - $\alpha'$  phases separation in 7–12 Cr martensitic steels, *J. Nucl. Mater.* 312 (2003) 236–248.
- [10] M. Miller, J. Bentley, APFIM and AEM investigation of CF8 and CF8M primary coolant pipe steels, *Mater. Sci. Technol.* 6 (1990) 285–292.
- [11] C. Pareige, S. Novy, S. SAILLET, P. Pareige, Study of phase transformation and mechanical properties evolution of duplex stainless steels after long term thermal ageing (>20 years), *J. Nucl. Mater.* 411 (2011) 90–96.
- [12] H.M. Chung, T.R. Leax, Embrittlement of laboratory and reactor aged CF3, CF8, and CF8M duplex stainless steels, *Mater. Sci. Technol.* 6 (1990) 249.
- [13] J.M. Vitek, S.A. David, D.J. Alexander, J.R. Keiser, R.K. Nanstad, Low temperature aging behavior of type 308 stainless steel weld metal, *Acta Mater.* 39 (1991) 503.
- [14] H.D. Newell, Properties and characteristics of 27% chromium-iron, *Metal. Prog.* 49 (5) (1946) 977–1006.
- [15] R. Kampmann, R. Wagner, Decomposition of Alloys: the Early Stages//Proc. 2nd Acta-scripta Metall. Conf., Pergamon, Oxford, 1984, pp. 91–103.
- [16] J.C. LaSalle, L.H. Schwartz, Further studies of spinodal decomposition in Fe-Cr, *Acta Metall.* 34 (1986) 989–1000.
- [17] F. Bley, Neutron small-angle scattering study of unmixing in Fe-Cr alloys, *Acta Metallurgica Materialia* 40 (1992) 1505–1517.
- [18] H.D. Solomon, L.M. Levinson, Mössbauer effect study of '475°C embrittlement' of duplex and ferritic stainless steels, *Acta Metall.* 26 (1978) 429–442.
- [19] M.K. Miller, J.M. Hyde, M.G. Hetherington, A. Cerezo, G.D.W. Smith, C.M. Elliott, Spinodal decomposition in Fe-Cr alloys: experimental study at the atomic level and comparison with computer models—I. Introduction and methodology, *Acta Metallurgica Materialia* 43 (1995) 3385–3401.
- [20] J.M. Hyde, M.K. Miller, M.G. Hetherington, A. Cerezo, G.D.W. Smith, C.M. Elliott, Spinodal decomposition in Fe-Cr alloys: experimental study at the atomic level and comparison with computer models—II. Development of domain size and composition amplitude, *Acta Metallurgica Materialia* 4 3 (1995) 3403–3413.
- [21] J.M. Hyde, M.K. Miller, M.G. Hetherington, A. Cerezo, G.D.W. Smith, C.M. Elliott, Spinodal decomposition in Fe-Cr alloys: experimental study at the atomic level and comparison with computer models—III. Development of morphology, *Acta Metallurgica Materialia* 43 (1995) 3415–3426.
- [22] J.E. Brown, An Atom Probe Study of the Spinodal Decomposition in Fe-Cr-Ni, University of Oxford, Oxford, UK, 1990.
- [23] G.T. Brown, R.T. Allsop, Embrittlement of a 12% Cr-4Ni steel, *J. Iron Steel Inst.* 194 (1960) 435–442.
- [24] P. Auger, F. Danoix, Atom probe and transmission electron microscopy study of aging of cast duplex stainless steels, *Mater. Sci. Technol.* 6 (1990) 300–313.
- [25] T. Hamaoka, A. Nomoto, K. Nishida, K. Dohi, N. Soneda, Accurate determination of the number density of G-phase precipitates in thermally aged duplex stainless steel, *Philos. Mag.* 92.22 (2012) 2716–2732.
- [26] C. Pareige, J. Emo, S. SAILLET, C. Domain, P. Pareige, Kinetics of G-phase precipitation and spinodal decomposition in very long aged ferrite of a Mo-free duplex stainless steel, *J. Nucl. Mater.* 465 (2015) 383–389.
- [27] U. Krupp, A. Giertler, M. Söker, H. Fu, B. Döonges, H.J. Christ, K. Istomin, A. Hüdecken, U. Pietsch, C.P. Fritzen, W. Ludwig, *Preced. Eng.* 74 (2014) 143–146.
- [28] O. Dmitrieva, D. Ponge, G. Inden, J. Millan, P. Choi, J. Sietsma, D. Raabe, Chemical gradients across phase boundaries between martensite and austenite in steel studied by atom probe tomography and simulation, *Acta Mater.* 59 (2011) 364–374.
- [29] D. Raabe, S. Sandlobes, J. Millan, D. Ponge, H. Assadi, M. Herbig, P.P. Choi, Segregation engineering enables nanoscale martensite to austenite phase transformation at grain boundaries: a pathway to ductile martensite, *Acta Mater.* 61 (2013) 6132–6152.
- [30] T. Hamaoka, A. Nomoto, K. Nishida, K. Dohi, N. Soneda, Effects of aging temperature on G-phase precipitation and ferrite-phase decomposition in duplex stainless steel, *Philos. Mag.* 92.34 (2012) 4354–4375.
- [31] Anon, ISO Designation 14556:2000: Steel-Charpy V-notch Pendulum Impact Test-Instrumented Test Method, Publication of ISO, 2000.
- [32] J. Piller, H. Wendt, Autocorrelation analysis of atom-probe concentration profiles, in: H.O. Andren, H. Norden (Eds.), Proc. Of 29th IFES, Almquistand Wiksell, Stockholm, 1982, pp. 265–274.
- [33] M.G. Hetherington, M.K. Miller, On the statistical analysis of atom-probe data, *J. Phys.* 48 (C6) (1987) 559–564.
- [34] C.J. Dalzell, Statistical analysis of an atom-probe study of iron chromium, *J. Phys.* 49 (C6) (1988) 411–414.
- [35] J. Emo, C. Pareige, S. SAILLET, C. Domain, P. Pareige, Kinetics of secondary phase precipitation during spinodal decomposition in duplex stainless steels: a kinetic Monte Carlo model-Comparison with atom probe tomography experiments, *J. Nucl. Mater.* 451 (2014) 361–365.
- [36] S.L. Li, Y.L. Wang, X.T. Wang, F. Xue, G-phase precipitation in duplex stainless steels after long-term thermal aging: a high-resolution transmission electron microscopy study, *J. Nucl. Mater.* 452 (2014) 382–388.
- [37] G. Kostorz, Phase Transformations in Materials, Wiley-VCH, Germany, 2001.
- [38] Tomo Ogura, Shoichi Hirotsawa, Alfred Cerezo, Tatsuo Sato, Atom probe tomography of nanoscale microstructures within precipitate free zones in Al-Zn-Mg (-Ag) alloys, *Acta Mater.* 58 (2010) 5714–5723.
- [39] S.L. Li, H.L. Zhang, Y.L. Wang, S.X. Li, K. Zheng, F. Xue, X.T. Wang, Annealing induced recovery of long-term thermal aging embrittlement in a duplex stainless steel, *Mater. Sci. Eng. A* 564 (2013) 85–91.